ResearchGate

See discussions, stats, and author profiles for this publication at: https://www.researchgate.net/publication/264268819

Charge Carrier Dynamics in a Ternary Bulk Heterojunction System Consisting of P3HT, Fullerene, and a Low Bandgap Polymer

ARTICLE *in* ADVANCED ENERGY MATERIALS · JULY 2013

Impact Factor: 16.15 · DOI: 10.1002/aenm.201201076

CITATIONS
29

READS
66

10 AUTHORS, INCLUDING:

Mauro Morana
Morphwize
28 PUBLICATIONS **2,714** CITATIONS
SEE PROFILE

Vito Sgobba
Bayerisches Zentrum für angewandte Ener…
40 PUBLICATIONS **1,743** CITATIONS
SEE PROFILE

Tayebeh Ameri
Friedrich-Alexander-University of Erlangen-…
72 PUBLICATIONS **2,020** CITATIONS
SEE PROFILE

Christoph J. Brabec
Friedrich-Alexander-University of Erlangen-…
398 PUBLICATIONS **25,571** CITATIONS
SEE PROFILE

Available from: Vito Sgobba
Retrieved on: 14 January 2016

Charge Carrier Dynamics in a Ternary Bulk Heterojunction System Consisting of P3HT, Fullerene, and a Low Bandgap Polymer

Markus Koppe, Hans-Joachim Egelhaaf, Ewan Clodic, Mauro Morana, Larry Lüer, Anna Troeger, Vito Sgobba, Dirk M. Guldi, Tayebeh Ameri, and Christoph J. Brabec*

The photoresponse of P3HT:$PC_{61}BM$ based organic solar cells can be enhanced by blending the bulk heterojunction with the low band gap polymer Si-PCPDTBT. Organic solar cells containing the resulting ternary blend as the photoactive layer deliver short circuit currents of up to 15.5 mA cm^{-2}. Morphological studies show modest phase separation without the perturbation of the crystallinity of the P3HT:$PC_{61}BM$ matrix, in accordance with the measured acceptable fill factors. Picosecond time-resolved pump-probe spectroscopy reveals that the sensitization of P3HT:$PC_{61}BM$ with Si-PCPDTBT involves the transfer of photogenerated positive polarons from the low band gap polymer to P3HT within few hundreds of picoseconds. Intensity dependent experiments in combination with global fitting show that the charge transfer from Si-PCPDTBT to P3HT competes with non-geminate charge carrier recombination of the holes in the Si-PCPDTBT phase with electrons in the $PC_{61}BM$ phase, both processes being of diffusive nature. At excitation densities corresponding to steady state conditions under one sun, modelling predicts hole transfer efficiencies exceeding 90%, in accordance with IQE measurements. At higher pump intensities, bimolecular recombination suppresses the hole transfer process effectively.

1. Introduction

Photovoltaic (PV) devices represent an important approach to meet the constantly growing global energy needs with renewable energy sources. Organic photovoltaic cells are an attractive alternative to other thin film PV technologies, due to their flexibility, light weight, variable colour, semitransparency, and potential low cost.[1] The present understanding of the working principle of bulk heterojunction single junction solar cells suggests an upper performance limit of ~ 12%.[2] OPV cells based on poly(3-hexylthiophen-2,5-diyl) (P3HT) in combination with [6,6]-phenyl-C_{61}-butyric acid methyl ester ($PC_{61}BM$) reach efficiencies of only 5%. The main reason is the poor match of the absorption spectrum of P3HT with the solar spectrum. Novel low-band gap polymers have been used to overcome this limitation. However, it has proven difficult to find polymers with the same advantageous charge extraction properties as those of P3HT. The majority of low-band gap polymers exhibits charge carrier recombination kinetics which are close to Langevin type behaviour. These polymers can therefore only be coated in thin films which in turn limits light absorption. Moreover, the absorption profiles of various recently presented low band gap materials[3–9] exhibit an absorption maximum in the 700–800 nm range but also have an absorption minimum which is typically located in the spectral region around 500 nm. A promising approach to reducing losses related to such absorption minima is blending the low band gap polymer with an additional component, which absorbs light significantly stronger in the region where the low band gap polymer has its absorption minimum. It has been shown in the past that the electron acceptor molecule (e.g., $PC_{71}BM$)[3,10] may represent such an additional component. However, for commercial applications this is not a viable option, due to the high cost of this material. Another possibility to overcome the limitations in light absorption while maintaining the advantageous charge transport properties of P3HT is the addition of a sensitizer polymer to form a ternary photoactive blend.[11–14] In a previous paper[13] we have shown that devices fabricated around the ternary bulk hetero-

Dr. M. Koppe, Dr. H.-J. Egelhaaf, E. Clodic, Dr. M. Morana
Konarka Austria F&E GmbH,
Altenbergerstr. 69, A-4040 Linz
E-mail: markus.koppe@jku.at
Dr. M. Koppe
Linz Institute for Organic Solar Cells (LIOS)
Johannes Kepler University of Linz
Altenbergerstr. 69, A-4040 Linz
Dr. H.-J. Egelhaaf
Belectric OPV GmbH, Landgrabenstr. 94, D-90443 Nürnberg
Dr. L. Lüer
IMDEA Nanociencia, C/Faraday, 9, E-28049 Cantoblanco
A. Troeger, Dr. V. Sgobba, Prof. D. M. Guldi
Institute for Physical Chemistry
Friedrich-Alexander University
D-91058 Erlangen
Dr. T. Ameri, and Prof. C. J. Brabec
imeet, Friedrich-Alexander University
D-91058 Erlangen
Prof. C. J. Brabec
Bavarian Center for Applied Energy Research (ZAE Bayern)
Am Weichselgarten 7, D-91058 Erlangen

DOI: 10.1002/aenm.201201076

© 2013 WILEY-VCH Verlag GmbH & Co. KGaA, Weinheim

junction P3HT:PC_{61}BM:C-PCPDTBT actually show enhanced photocurrents with respect to the binary blends P3HT:PC_{61}BM while the open circuit voltage of the ternary device is identical to that of a P3HT:PC_{61}BM device. However, due to losses in fill factor, device efficiencies exhibited only marginal improvements. These losses have been shown recently to be due to the deterioration of electron transport properties as a consequence of reduced crystallinity of the fullerene phase upon addition of C-PCPDTBT to the P3HT:PC_{61}BM blend.[15,16] A recently published paper[14] shows that blending the low band gap material poly[(4,4′-bis(2-ethylhexyl)dithieno[3,2-b:2′,3′-d]silole)-2,6-diyl-alt-(4,7-bis(2-thienyl)-2,1,3-benzothiadiazole)-5,5′-diyl] (Si-PCPDTBT)[5,17] with the wide band gap polymer system containing P3HT/PC_{61}BM not only results in significantly higher short circuit currents compared to the corresponding binary polymer/fullerene systems but actually enhances photovoltaic efficiencies by up to 25%. In contrast to the carbon-bridged analogue, Si-PCPDTBT does not perturb the advantageous morphology of the P3HT:PC_{61}BM blend which results in almost unaffected fill factors even at weight fractions of the low band gap polymer of 40%.

For the ternary blend system P3HT/C-PCPDTBT/PC_{61}BM we were able to show by steady-state photo-induced absorption spectroscopy that the photoinduced holes are exclusively localized on P3HT. This makes it plausible that the sensitization effect of the low band gap polymer is due to the transfer of photo-generated holes to the wide band gap polymer P3HT,[13] whose HOMO (E_{HOMO}(P3HT) = −5.1 eV) is shallower with respect to the HOMO of C-PCPDTBT (E_{HOMO}(C-PCPDTBT) = −5.3 eV).[18] This picture is corroborated by a recent pump-probe spectroscopic study, which has revealed that at C-PCPDTBT weight fractions below 10% the positive charge carriers photogenerated in the low band gap polymer are efficiently transferred to the P3HT domains.[19] At higher contents of C-PCPDTBT, increasing fractions of charge carriers recombine within the low band gap polymer due to decreasing rates of transfer to P3HT. In this work we elucidate the underlying mechanism of the efficient photocurrent enhancement in P3HT:Si-PCPDTBT:PC_{61}BM devices in more detail by employing pump-probe spectroscopy with sub-picosecond time resolution, exciting Si-PCPDTBT exclusively (at 785 nm) and monitoring the dynamics of the excited species in both polymers. We will show that sensitization by the low band gap material Si-PCPDTBT is highly efficient because even at high weight fractions of the low band gap polymer the transfer of the photo-generated polarons onto the hole transport material P3HT is completed within few hundreds of picoseconds.

2. Results and Discussion

2.1. Device Performance

In order to quantify the effect of the sensitizer polymer on device efficiency, the ternary blend cell is compared to the two binary polymer/PC_{61}BM cells. All the reported cells are of regular architecture (see Experimental Section). P3HT/PC_{61}BM reference devices deliver short circuit currents in the range of about 10 mA cm^{-2}. With a fill factor of 60% and an open circuit voltage of 560 mV the P3HT reference devices have an efficiency of close to 3.5%. P3HT/PC_{61}BM devices are thermally annealed, resulting in the well known performance enhancement.[20] The optimum active layer thickness is found to be in the range of 180–200 nm. Smaller thicknesses result in short circuit current losses whereas thicker active layers yield reduced fill factors which are not compensated by the slightly increased short circuit currents. Si-PCPDTBT/PC_{61}BM reference devices deliver short circuit currents of 11.6 mA cm^{-2} and open circuit voltages of 600 mV. Due to lower fill factors (~ 50–52%) the overall performance is comparable to P3HT. Thermal treatment does not have a significant effect on performance. The optimum active layer thickness of these devices is found to be around 140 nm. For thicker devices severe losses of fill factors are observed. (FF < 40% are obtained for active layer thicknesses comparable to those of P3HT/PC_{61}BM devices).

The comparison of the absorption profiles of the binary and the ternary blends (**Figure 1** a) reveals the two major reasons for blending Si-PCPDTBT into the binary P3HT/PC_{61}BM blend. On one hand, the low band gap material Si-PCPDTBT extends the photoresponse of the blend into the near infrared (NIR) region up to 830 nm. On the other hand, P3HT compensates for the low extinction coefficient of Si-PCPDTBT in the 500 nm region. Correspondingly, devices based on P3HT/Si-PCPDTBT/PC_{61}BM ternary blends have the potential for efficiencies which are significantly enhanced over those of the two reference systems. In order to obtain blend systems which actually exploit this potential and are thus apt for the spectroscopic investigations, the devices were optimized with respect to blend composition and layer thickness. More extensive optimization procedures are beyond the scope of this paper and are described elsewhere.[14]

The optimum P3HT/Si-PCPDTBT ratio in the P3HT/Si-PCPDTBT/PC_{61}BM ternary blend is determined to be 7/3. For lower Si-PCPDTBT contents the resulting short circuit currents are negatively affected whereas higher Si-PCPDTBT contents have a negative influence on the fill factor. The optimum polymer-mix/fullerene ratio, mainly impacting the fill factor of ternary blend devices, is found to be 1:1.3 resulting in an optimum ternary blend composition of 0.7/0.3/1.3 P3HT/Si-PCPDTBT/PC_{61}BM. The optimized active layer thickness is in the range of 250 nm. Thermal annealing of ternary blend devices shows a beneficial effect on the overall device performance, similar as described before for P3HT/PC_{61}BM devices. Maximum current densities delivered by the ternary blend devices are 15.5 mA cm^{-2}, corresponding to a 50% increase compared to the current densities delivered by the binary P3HT/PC_{61}BM devices. This increase results in a clear enhancement of device performance with respect to the binary blends, despite the somewhat lower fill factors (see below). From the values of EQE (Figure 1b) and absorbance in the absorption band of Si-PCPDTBT ($OD_{@780\,nm}$ = 0.24) an IQE of about 90% is obtained over the whole band. Open circuit voltages are comparable to P3HT/PC_{61}BM devices (560 mV). Fill factors (FF) are reduced with respect to P3HT/PC_{61}BM devices of the same thickness. They increase with decreasing ternary blend film thicknesses but never exceed 53%, due to the relatively large film thicknesses used in this study. We ascribe the FF loss at increased Si-PCPDTBT contents

© 2013 WILEY-VCH Verlag GmbH & Co. KGaA, Weinheim
Adv. Energy Mater. 2013,
DOI: 10.1002/aenm.201201076

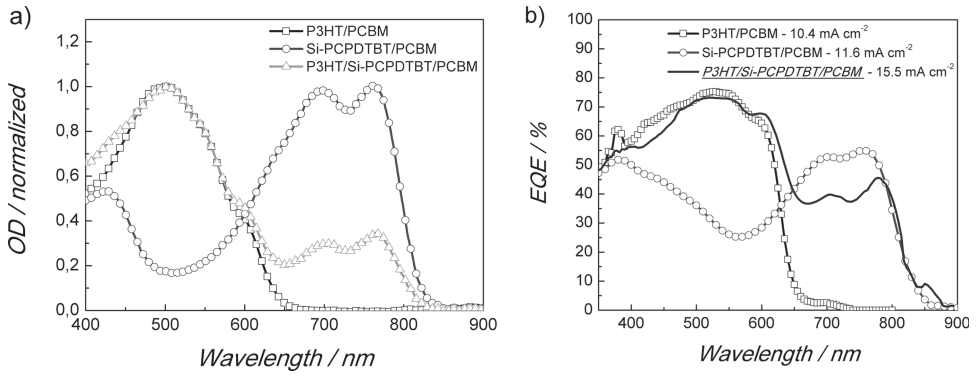

Figure 1. a) Normalized absorption spectra of P3HT/$PC_{61}BM$ (1/1) (squares), Si-PCPDTBT/$PC_{61}BM$ (1/1) (circles) and P3HT/Si-PCPDTBT/$PC_{61}BM$ (0.7/0.3/1) (triangles). b) External quantum efficiencies (EQE) of devices based on P3HT/$PC_{61}BM$ (1/1–squares), Si-PCPDTBT/$PC_{61}BM$ (1/2–circles) and P3HT/Si-PCPDTBT/$PC_{61}BM$ blends (0.7/0.3/1.3–solid line)

to the formation of unfavourable film morphologies, similar to the situation in ternary devices with C-PCPDTBT.[15,16] We will show in the subsequent morphology section that also the vertical structure of the bulk morphology is a possible reason for the reduced fill factors.

2.2. Morphology

Phase separation of binary and ternary polymer mixtures has been extensively studied in the last couple of years. Since most polymer mixtures tend to phase separate, good miscibility is rarely observed. A multitude of parameters like polymer molecular weight, which affects the entropy of mixing, differences in wetting behaviour, induced by variations of surface energies, as well as the processing conditions have a strong influence on the demixing behaviour of blended polymer systems. Device preparation by spin coating or doctor blading at elevated temperatures involves a fast drying process of thin polymer wet films, which induces a fast immobilization of the polymer chains. Thus the system is "frozen" in a non-equilibrium morphology instead of reaching the thermodynamically stable state. This effect, also called solvent quenching, is well known from non-conjugated polymer-polymer blends.[21] For conjugated polymer systems this effect is commonly used to adjust a certain domain size, corresponding to a certain demixing behaviour.[22–24] Modelling the phase formation of conventional polymer-polymer blends suggests the formation of stratified phases in the early stages of drying.[25,26] If this vertical stratification is maintained throughout the drying process, the enrichment of one of the polymers at the film surface is commonly observed for conventional polymer/polymer blend systems[27,28] as well as for conjugated ones.[29–31] If this layered structure cannot be maintained till the film drying is completed, lateral domains are formed due to interfacial instabilities as shown for conjugated polymer-polymer mixtures.[30,32,34,35] In order to check the three dimensional demixing behaviour of the two polymers P3HT and Si-PCPDTBT, morphological studies by atomic force microscopy (AFM) and time-of-flight secondary-ion-mass-spectrometry (TOF-SIMS) were performed on the active layers of photovoltaic devices. (Additional information about TOF-SIMS are given in the experimental section)

Figure 2a and b show the AFM scans of the two binary blends P3HT/$PC_{61}BM$ (1/1) and Si-PCPDBTB/$PC_{61}BM$ (1/1) in a 5 × 5 µm section. Both images do not show any signs of significant lateral phase separation involving surface modification. The surfaces of all investigated Si-PCPDTBT/$PC_{61}BM$ layers are significantly rougher than those of P3HT/$PC_{61}BM$ layers. Blending P3HT/$PC_{61}BM$ with various ratios of Si-PCPDTBT does not significantly modify the structure of the surface.

The surface roughnesses of a broad range of polymer/polymer ratios (9/1–1/9; fullerene content constant) are comparable to those of Si-PCPDTBT/$PC_{61}BM$ layers. Varying the fullerene content (from fullerene/polymer ratios of 1/1 to 1.3/1 w/w) also does not have a noticeable impact on the surface morphology. These observations indicate that also in the ternary blends there is no large scale lateral phase separation which would involve major rearrangements of the sample surface.

In order to check to which extent vertical phase separation is present in the investigated ternary blends, TOF-SIMS measurements were performed. No vertical phase separation or gradients are observed for the two binary systems P3HT/$PC_{61}BM$ (1/1) and Si-PCPDTBT/$PC_{61}BM$ (1/1) (**Figure 3**a and b). The rising edges at the surfaces represent the initial stabilisation phase of the sputtering process. The distribution of sulphur in Figure 3a is attributed to P3HT molecules, the distribution of sulphur and silicon in Figure 3b is attributed to Si-PCPDTBT.

The oxygen distributions in all three profiles (Figure 3a-c) indicate that the vertical fullerene distribution in the active layers is homogeneous in all three cases. To distinguish between the two donor-polymers in the ternary blend the silicon atom distribution is invoked. As shown in Figure 3c, a slight Si-PCPDTBT enrichment in the top 5 nm of the ternary blend layer is observed. The subjacent layer, which takes up about half of the volume of the whole bulk, consists of a Si-PCPDTBT poorer region. In the lower half of the ternary bulk all three components are distributed homogeneously. The sulphur and the oxygen distributions in the ternary layer show no gradients between the polymer/polymer and the fullerene phase, except for the region close to the surface.

© 2013 WILEY-VCH Verlag GmbH & Co. KGaA, Weinheim

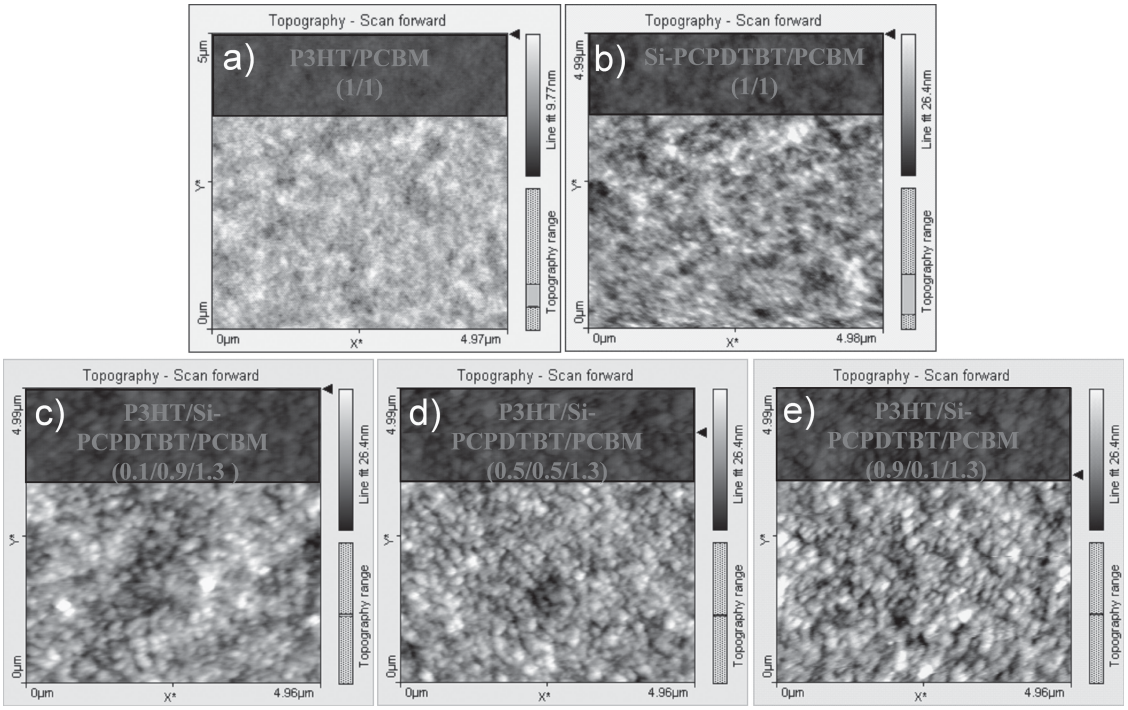

Figure 2. AFM scans (5 × 5 µm) of following blends: a) P3HT/$PC_{61}BM$ (1/1), b) Si-PCPDTBT/$PC_{61}BM$ (1/1), c) P3HT/Si-CPDTBT/$PC_{61}BM$ (0.1/0.9/1.3) d) P3HT/Si-CPDTBT/$PC_{61}BM$ (0.5/0.5/1.3) e) P3HT/Si- CPDTBT/$PC_{61}BM$ (0.9/0.1/1.3). All layers are thermally annealed.

2.3. Charge Carrier Dynamics

In order to obtain a more detailed insight into the photophysical steps underlying the sensitization process in the ternary P3HT:Si-PCPDTBT:$PC_{61}BM$ blend, we employ pump-probe spectroscopy on the picosecond time scale, which allows us to follow the fate of excitons and charges upon selective excitation of the low band gap polymer. In **Figure 4**a and b, we show femtosecond pump-probe spectra during the first 4 picoseconds after selective photoexcitation of Si-PCPDTBT at 785 nm, for the binary and the ternary blend, respectively. The pump-probe spectra recorded immediately (200 fs) after the pump pulse are very similar for both the binary and ternary blends: there is a photoinduced absorption (PA) band around 500 nm, which we assign to singlet excited state absorption, in analogy to the assignment of the band at the same wavelength in C-PCPDTBT.[19,33] It is neighboured by a strong band with positive ΔT/T values from 540 nm to at least 730 nm, where the spectral window of our visible probe pulse ends. Since this band coincides with the ground state absorption of the Si-PCPDTBT phase, we associate it with transient ground state bleaching (GB), confirming that the primary excitation dwells in the Si-PCPDTBT phase. In the near infrared (NIR) spectral region, we find a strong PA band at 1400–1500 nm, and a positive band around 900 nm, superposed by a large PA band covering the spectral region from 850 to 1300 nm. Due to this superposition, most or all (for both the binary and ternary blend) of this positive band occurs actually at negative ΔT/T values. On a time scale of few picoseconds, a significant evolution of the pump-probe spectra takes place. In both, the binary and the ternary blends, the PA band at 1400 nm and the positive band at 900 nm disappear within 4 ps. After 4 ps, the dominant feature in the NIR spectral region for both blends is a PA band around 1300 nm. In the ternary blend, an additional smaller PA band around 1000 nm is observed. The inset of Figure 4a shows that the positive band at 920 nm and the PA band at 1400 nm decay with the same kinetics, which indicates that both bands probe the same photophysical species. We assign the positive band at 920 nm to stimulated emission from the first excited singlet state S_1 of the Si-PCPDTBT phase, and the PA at 1400 nm to an S_1-S_n transition from the same state. Hence, our data suggest that in both blends, quenching of the Si-PCPDTBT exciton occurs within approximately one picosecond. The high value of the IQE in the binary blend indicates that exciton quenching results mostly in charged states, excluding any significant generation of triplet or immobilized charge transfer states. We therefore assign the PA band at 1300 nm to the $D_2 \leftarrow D_0$ transition of the polaron in Si-PCPDTBT, in analogy to the assignment of the PA band around 1200 nm in C-PCPDTBT.[34] It is interesting to note that in the binary blend (Figure 4a), the polaron band at 1300 nm is already fully developed at the end of the pump pulse. This is consistent with the finding, obtained e.g. in binary P3HT:$PC_{61}BM$ blends, that a large portion of the photoinduced charges is actually formed on the subpicosecond time scale.[21,35,36] Our spectra confirm this picture also for the system Si-PCPDTBT:$PC_{61}BM$. A comparison of the spectral evolution in the ternary blend with that in the binary blend Si-PCPDTBT:$PC_{61}BM$ (Figure 4a and b) shows clear evidence of a delayed transfer of excited states from Si-PCPDTBT into the P3HT phase: a positive band around 540 nm

© 2013 WILEY-VCH Verlag GmbH & Co. KGaA, Weinheim

DOI: 10.1002/aenm.201201076

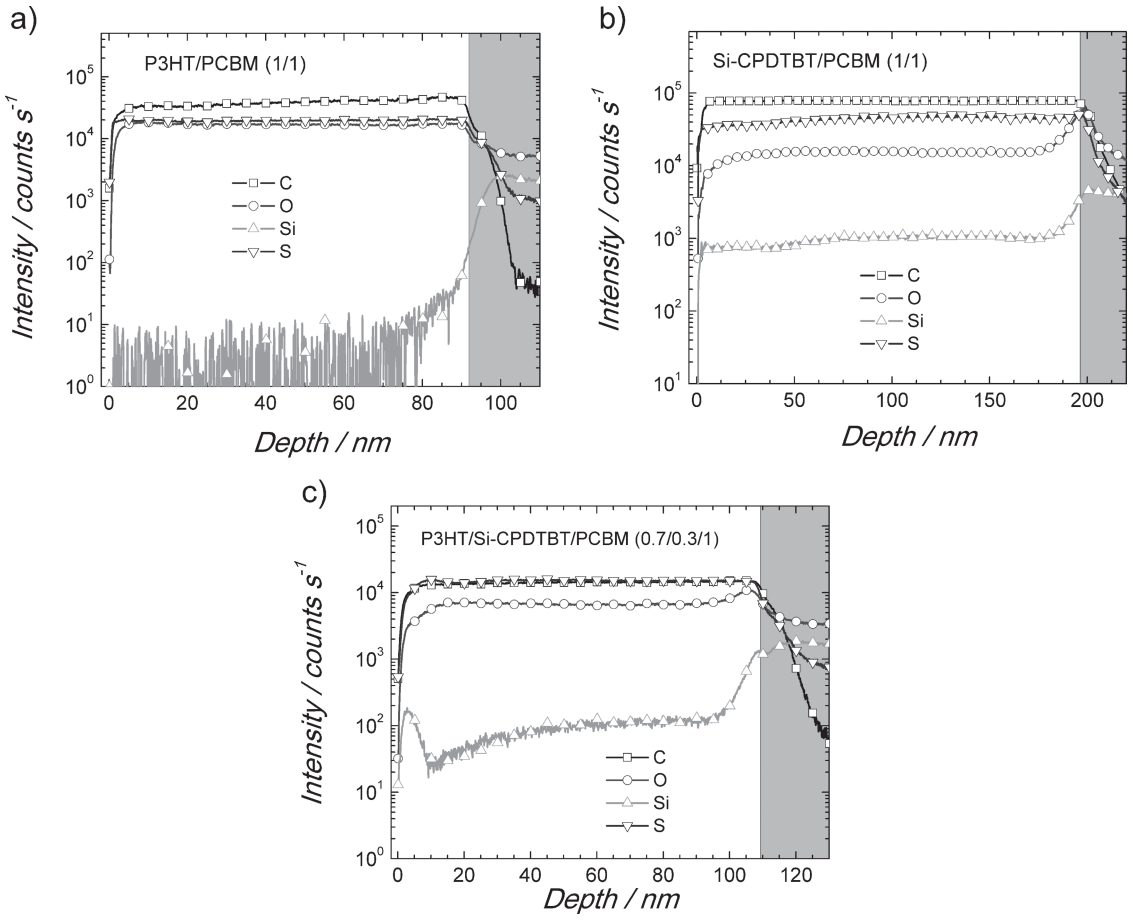

Figure 3. TOF-SIMS profiles of thermally annealed layers containing a) P3HT/$PC_{61}BM$ (1/1) b) Si- PCPDTBT/$PC_{61}BM$ (1/1) and c) P3HT/Si-PCPDTBT/$PC_{61}BM$. The tracing of the four atoms C, O, S and Si is shown. The grey-filled rectangle represents the glass substrate.

rises over time, assigned to the bleaching of the P3HT ground state absorption, together with the observation of an additional band around 1000 nm, which is well-known as the $D_2 \leftarrow D_0$ polaron absorption of P3HT.[37] Note however that even at times as early as 0.34 ps, the typical vibronic structure of the P3HT bleach can clearly be observed; this ultrafast appearance of the P3HT bleach is confirmed for all the pump intensities applied in this work, see **Figure 5**b. The reason for the bleach is most probably an ultrafast hole transfer at the Si-PCPDTBT/P3HT interface after direct formation of electrons and holes in the Si-PCPDTBT phase. Exciton or charge formation in P3HT under these conditions (pumping at 780 nm) occurs to a much lesser extent (data not shown).

In summary, the following qualitative picture emerges for the elementary photophysics in ternary Si-PCPDTBT:P3HT:$PC_{61}BM$ blends on the timescale of four picoseconds: photoexcitation at 785 nm creates predominantly neutral Si-PCPDTBT excitons, that are quenched at the Si-PCPDTBT:$PC_{61}BM$ interface within about one picosecond to form polarons. A significant portion of P3HT and Si-PCPDTBT polarons is formed in even less than 200 fs. Subsequently, mobile Si-PCPDTBT positive polarons cross the boundary between Si-PCPDTBT and P3HT.

Figure 5a shows pump-probe spectra of the ternary blend measured at low pump intensity over the time scale of 400 ps. Owing to the spectral congestion in the near infrared (NIR) region, we focus exclusively on the visible part of the spectrum. At 540 nm, the Si-PCPDTBT related PA and GB dynamics cancel each other, so that at this wavelength, the dynamics of the P3HT GB band can be detected selectively. The delayed build-up of the GB in the P3HT region at 540 nm can be observed clearly, being completed in little more than 100 ps. The kinetics of the P3HT bleach build-up is identical to those of the Si-PCPDTBT bleach recovery for all pump intensities (Figure 5b). However, from the inspection of Figure 5, it is obvious that the spectral weight of the final P3HT bleach after 100 ps is much smaller than the initial spectral weight of the Si-PCPDTBT bleach. In Figure 5b, this has been taken into account by the scaling factors of the Si-PCPDTBT spectra, which strongly vary with pump intensity.

Obviously, under the experimental conditions of Figure 5a, most of the Si-PCPDTBT bleach recovery is not caused by polaron transfer towards P3HT, but by an intensity dependent loss process, most probably non-geminate polaron recombination at the Si-PCPDTBT:$PC_{61}BM$ interface. Under light intensities according to irradiation by 1 sun, this latter process is strongly suppressed, as demonstrated by the high IQE values of more than 90% observed upon excitation of ternary blend devices at 780 nm (Figure 1). Unfortunately, quantitative studies on charge

© 2013 WILEY-VCH Verlag GmbH & Co. KGaA, Weinheim

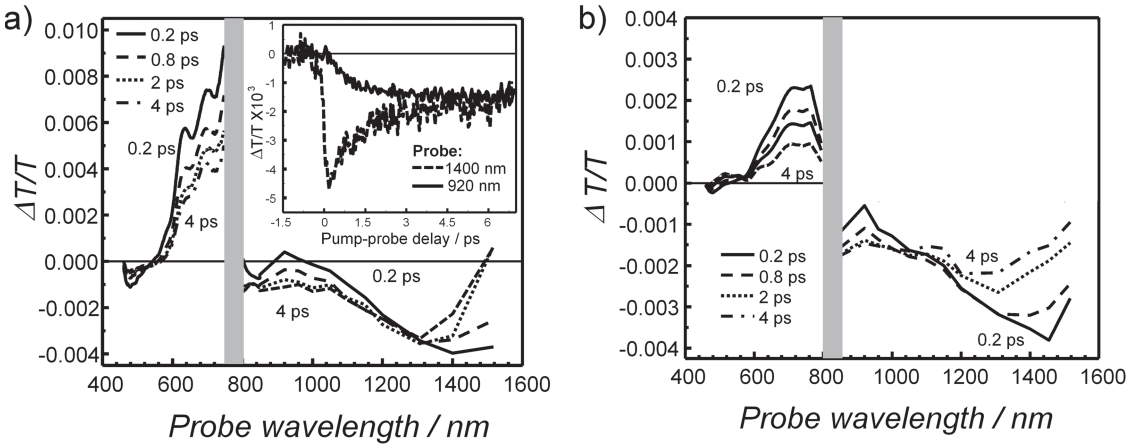

Figure 4. Pump-probe spectra of films of the binary blend Si-PCPDTBT/$PC_{61}BM$ (1/1) a) and the ternary blend P3HT/Si-PCPDTBT/$PC_{61}BM$ (0.7/0.3/1) b) after pumping at 785 nm. The spectra in the NIR spectral region were obtained by pumping with pulse energies of 7$\mu J \cdot cm^{-2}$. The spectra in the visible region were excited using pulse energies of 70$\mu J \cdot cm^{-2}$. They are normalized to the NIR traces in the overlap region. Inset of (a): time traces at 920 nm and 1400 nm.

transfer processes in the picoseconds time-scale under 1 sun conditions are hindered by high noise level. Here we pursue a different strategy: varying the pump intensity over a large range allows us to disentangle intensity-dependent non-geminate polaron recombination from intensity-independent polaron transfer between the phases, and to obtain the respective rate constants by a global fitting routine. These rate constants are then used to predict the dynamics of polaron transfer into the P3HT phase at irradiation conditions of 1 sun. The corresponding rate Equations of the polaron dynamics are based on the following reasoning. The negative differential absorption at 633 nm is almost entirely due to the bleach of Si-PCPDTBT (because at this wavelength, the P3HT polaron and the P3HT PA contributions cancel each other), while the negative differential absorption at 540 nm is dominated by the bleach of P3HT (a small and constant contribution of PA from Si-PCPDTBT at 540 nm is subtracted). We denote the bleach at 633 nm by S, while we denote the bleach at 540 nm, corrected for the PA contribution of Si-PCPDTBT, by P. The bleach P is entirely caused by P3HT polarons, since excitons cannot be transferred from the Si-PCPDTBT phase into the P3HT phase (due to the wider optical "band gap" of the latter), nor are they generated resonantly by any significant amount. In contrast, the bleach S can be caused by charges as well as by singlet states. However, since the latter have only a lifetime of about one picosecond, we disregard their contribution to S in the kinetic modelling. Both P and S are then directly proportional to the concentration of charged states in P3HT and Si-PCPDTBT, respectively, where the proportionality is given by Beer-Lambert's law. We thus arrive at the following set of rate Equations for the dynamics of S and P:

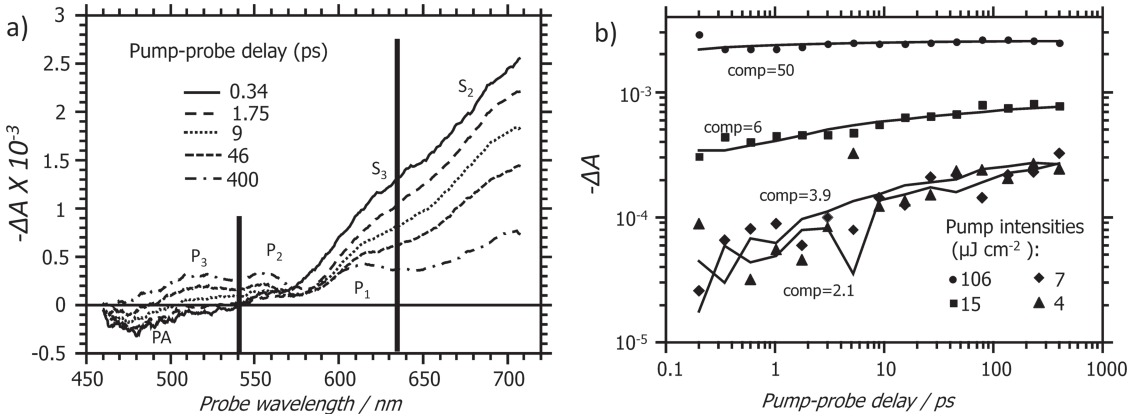

Figure 5. a) Differential absorption spectra of the ternary blend, measured at the low pump intensity of 7 μJ cm^{-2} at different time delays. The vibronic progression of the Si-PCPDTBT bleach is denoted S_x, while that of the bleach of P3HT is denoted P_x. The PA contribution of Si-PCPDTBT is also indicated. A clear build-up of P3HT related features is observed. Vertical bars indicate probe energies where the dynamics are nearly exclusively defined by Si-PCPDTBT and P3HT, respectively. b) Dynamics of differential absorption taken at 540 nm (symbols) after proper subtraction of the PA contribution to the signal. The lines are y-compressed, y-shifted and y-inverted replica of differential absorption dynamics taken at 633 nm. The compression factors of the traces at 633 nm, needed to yield satisfactory superposition, are given for all pump intensities.

© 2013 WILEY-VCH Verlag GmbH & Co. KGaA, Weinheim

DOI: 10.1002/aenm.201201076

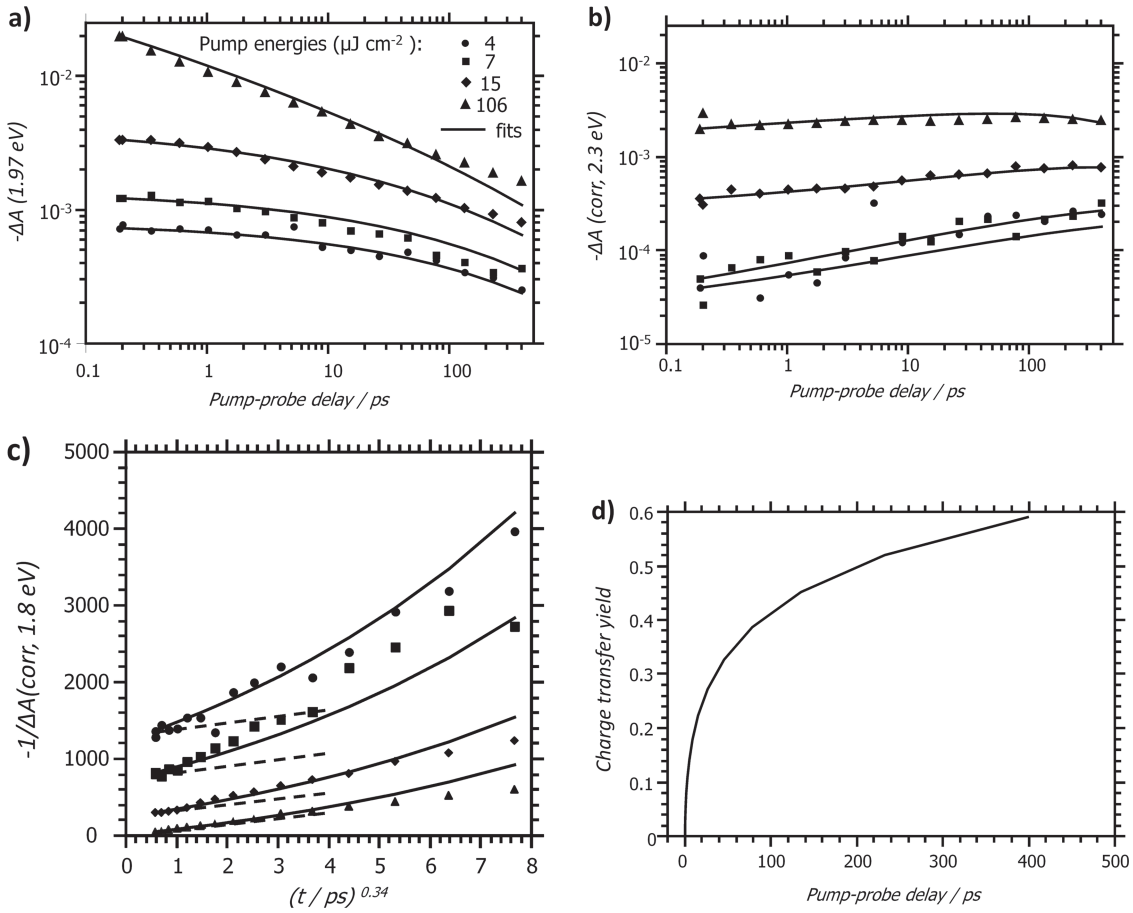

Figure 6. Differential absorption kinetics (obtained from ΔT/T, using the low signal approximation) at four different pump energies and two different probe wavelengths (data points) and global fits (lines) according to Equation 1 and 2. a) Differential absorption at 633 nm (Si-PCPDTBT bleach) b) Differential absorption kinetics at 540 nm corrected by the subtraction of a small contribution of PA band of Si-PCPDTBT to yield "pure" GB of P3HT. c) Same as a), but given on a reciprocal y axis against $t^{0.34}$. In this representation, contribution of bimolecular polaron recombination in Si-PCPDTBT phase is a straight line (dashed lines). d) Temporal development of the quantum yield of transfer of photo-excited charge carriers from Si-PCPDTBT to P3HT at excitation densities under 1 sun conditions, calculated by Equation 4 using the data of Table 1.

$$-\frac{dS}{dt} = k_1(t)\cdot S + k_2(t)\cdot S^2 \quad (1)$$

$$\frac{dP}{dt} = r\cdot k_1(t)\cdot S - k_4 P^2 \quad (2)$$

where the rate coefficient for charge transfer from the Si-PCPDTBT phase to the P3HT phase is $k_1(t) = k^*_1 \cdot t^{-\gamma}$, and the rate coefficient for the bimolecular charge recombination in the Si-PCPDTBT phase is $k_2(t) = k^*_2 \cdot t^{-\gamma}$. Since both processes are diffusion mediated, we choose a time dependent expression for both rate coefficients using the same exponent of γ. The rate constant k_4 considers charge carrier recombination in P3HT. Bimolecular polaron recombination in the P3HT phase was included into the model since the presence of this contribution resulted evident by increasing pump intensity. The parameter r in Equation 2 takes into account the different contributions of charges to ground state bleaching in the Si-PCPDTBT and P3HT phases. The fits are shown in **Figure 6**. We find that a single set of parameters given in **Table 1** successfully reproduces the dynamics of both S and P over an intensity range of a factor of 25. First, we discuss the exponent γ. For purely one-dimensional diffusion, an exponent of $\gamma = -0.5$ is expected. The stronger negative exponent that we find here is explained by diffusion kinetics with a charge carrier mobility which decreases during energetic relaxation, a generally occurring phenomenon in disordered films. Since the quantities P and S are differential absorptions and thus unitless, the units of k_1 and k_2 are both $ps^{-0.34}$. To rationalize these values, let us consider two limiting

Table 1. Spectroscopic rate constants from a global fit of rate Equation 1 and 2 to the experimental data.

Parameter (units)	k^*_1 ($ps^{-0.34}$)	k^*_2 ($ps^{-0.34}$)	r	γ	κ_4
value	0.043	23.4	0.364	–0.66	0.372

© 2013 WILEY-VCH Verlag GmbH & Co. KGaA, Weinheim

cases. For very high pump intensities, bimolecular annihilation will dominate the decay of S. Setting k_1 to zero in Equation 1, integration yields:

$$\frac{1}{S(t)} = \frac{1}{S_0} + \frac{k_2^*}{1-\gamma} t^{-\gamma+1} \quad (3)$$

Since the global fit results in a value for $\gamma = 0.66$, it follows from Equation 3 that plotting 1/S(t) against $t^{0.34}$ will result in straight lines with a pump intensity independent slope of about 31 $ps^{-0.34}$ (dashed lines in Figure 6c). We find that at the highest pump energy of 106 μJ cm^{-2}, the initial slope of the experiment is well reproduced by Equation 3, showing that bimolecular recombination dominates the early kinetics. At lower intensities, the slope of the reciprocal differential absorptions is significantly higher than predicted by Equation 3, showing that bimolecular recombination is only a minor contribution, even at early times. At very low intensities, we can set $k_2 = 0$ and obtain after integration

$$S(t) = S_0 \cdot \exp\left(-\frac{k_1^0}{1-\gamma} t^{-\gamma+1}\right) \quad (4)$$

Equation 4 predicts that in the absence of bimolecular recombination, 50%, 80% and 90% of the charges are transferred from the Si-PCPDTBT phase to the P3HT phase within 145, 1650 and 4900 ps after the pump pulse, respectively (Figure 6d). These numbers slightly deviate from the numerical fits in Figure 6d; this deviation is caused by the assumption of a delta pulse for exciton generation in the analytical treatment, yielding an infinite slope for the polaron generation for t = 0. The total yield of charge transfer under 1 sun irradiation (i.e. the proportion of polarons that is transferred towards P3HT before undergoing bimolecular recombination in the Si-PCPDTBT phase) can be calculated by using the rate coefficients in Table 1. To this end, we re-state Equation 1 for stationary state conditions under continuous irradiation:

$$g = -k_1(t) \cdot S_{st} - k_2(t) \cdot S_{st}^2 \quad (5)$$

where g denotes the continuous wave (CW) generation term of polarons in Si-PCPDTBT, and S_{st} is the stationary Si-PCPDTBT bleach at 690 nm caused by the stationary polaron population. If only charge transfer (by k_1) and bimolecular recombination (by k_2) need to be considered, then the charge transfer yield is given by:

$$\varphi_{CT} = \frac{k_1^*}{k_1^* + S_{st} \cdot k_2^*} \quad (6)$$

Since the time dependence of both k_1 and k_2 has been assumed equal (justified by the reasonable fitting results and the common reason for the time dependence of both, namely diffusion and mobility dispersion, only the time-independent constants remain. Using the values from Table 1 and $S_{st}(@1sun) = 7 \cdot 10^{-5}$, (at 633 nm), we obtain $\phi_{CT} \approx 0.97$, explaining the high values of IQE upon excitation of Si-PCPDTBT in ternary blend devices (Figure 1).

3. Conclusion

In conclusion, we have shown by picosecond pump-probe spectroscopy that the effective sensitization of bulk heterojunction solar cells based on P3HT:PC_{61}BM blends by addition of Si-PCPDTBT is based on the rapid transfer of photo-generated positive polarons from the Si-PCPDTBT phase to the P3HT phase, leading to the depletion of the hole population on the low band gap polymer within few hundreds of picoseconds after the pump pulse (schematically shown in **Figure 7**). The transfer time of few hundreds of picoseconds suggests that there is no large scale phase separation between the two polymers, which is also in line with the atomic force micrographs of the ternary blends. As the quantitative evaluation of the spectrally congested near infrared region proved to be prone to arbitrariness, the ground state bleaching signals of the two polymers were invoked for enhanced precision. Intensity dependent experiments in combination with global fitting show that the charge transfer from Si-PCPDTBT to P3HT competes with non-geminate charge carrier recombination of the holes in the Si-PCPDTBT phase with electrons in the PC_{61}BM phase, both processes being of diffusive nature. At excitation densities corresponding to steady state conditions under one sun, modelling predicts hole transfer efficiencies exceeding 90%, in accordance with IQE measurements. At higher pump intensities, bimolecular recombination suppresses the hole transfer process effectively.

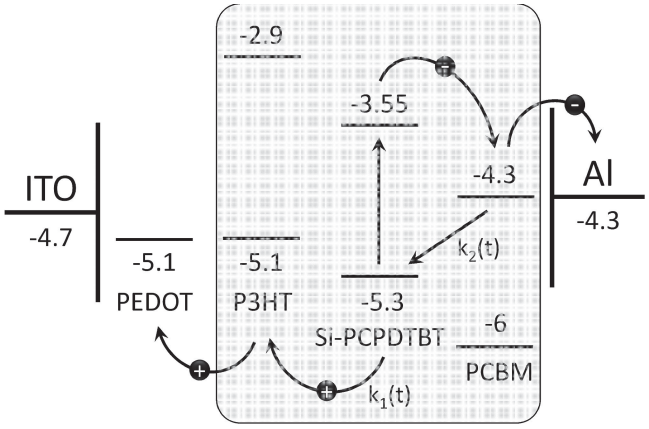

Figure 7. Energy level scheme of the ternary blend device ITO/PEDOT:PSS/P3HT:Si- PCPDTBT:PC_{61}BM/Al. Photophysical processes upon excitation of the low band gap polymer are indicated by arrows.

The observed efficient hole transfer from the low band gap polymer to the wide band gap polymer explains why the short circuit current of P3HT:PC_{61}BM devices increases upon the addition of Si-PCPDTBT while the open circuit voltage remains unaffected. The fill factors of the ternary P3HT:Si-PCPDTBT:PC_{61}BM blend are significantly higher than those in the corresponding blend P3HT:C-PCPDTBT:PC_{61}BM of the carbon analogue, but slightly reduced compared to the binary P3HT:PC_{61}BM reference system. This has been explained by the lesser perturbation of the crystalline structure of the bulk heterojunction upon admixture of Si-PCPDTBT than in the case of C-PCPDTBT.[14,16] Lower fill factors with respect to P3HT:PC_{61}BM devices might originate from ~ 60 nm larger active layer thicknesses in the optimized ternary blends. Our TOF-SIMS studies, which show a slight vertical phase separation suggest an additional reason for the low fill factors. The

© 2013 WILEY-VCH Verlag GmbH & Co. KGaA, Weinheim

DOI: 10.1002/aenm.201201076

measurements of ternary active layers show that up to 1/3 of the overall active layer volume consists of a Si-PCPDTBT-poor layer. This Si-PCPDTBT-poor layer is not placed right at one of the bulk interfaces but close to the electron injection electrode spaced with an about 20 nm thick slightly Si-PCPDTBT enriched layer. Since positive polarons can be easily transferred from Si-PCPDTBT onto P3HT but not the other way round, this ~ 20 nm layer may act as a kind of barrier for holes.

4. Experimental Section

Devices of the general regular structure glass/ITO/PEDOT:PSS/photoactive layer/LiF/Al were prepared as described in reference.[38] All devices are thermally annealed at 140 °C for 4 minutes. Photovoltaic layers contained P3HT (purchased from Rieke Inc.; number-average molecular weight 25 000 g mol^{-1}, weight-average molecular weight 50 000 g mol^{-1}; RR = 93%), Si-PCPDTBT (number-average molecular weight 25 000 g mol^{-1}, weight-average molecular weight 50 000 g mol^{-1}) and the methanofullerene $PC_{61}BM$ in various ratios as mentioned. The variations of active layer thicknesses of each series of devices were within the range of typical active layer surface roughness. Absorbance measurements of polymer/fullerene layers were performed with a Perkin Elmer 35 UV-VIS spectrometer. The current–voltage characteristics were measured using a Keithley 2400 SMU while the solar cells were illuminated under AM1.5G irradiation by an Oriel Xenon solar simulator (100 mW cm^{-2}). EQEs were measured by using lock-in amplifier (SR830, Stanford Research Systems) with current preamplifier (HMS-74) under short circuit condition. The devices were illuminated by monochromatic light from a xenon lamp passing through a monochromator (Oriel Cornerstone) with a typical intensity of a few µW. Between the Xenon lamp and the monochromator a mechanical chopper was mounted. Chopping frequencies in the range of 10–200 Hz were applied. A calibrated silicon diode (Hamamatsu S2281) was used as a reference. AFM measurements were performed with a Nanosurf Easy Scan 2 in contact mode. The surface scans were carried out at devices which were used for jV-characterisation. For thickness measurements of the active layers the samples were scratched and the height profile was detected.

The technique of secondary ion mass spectrometry (SIMS) is one of the most sensitive and commonly-employed surface analytical techniques. It offers a high lateral resolution (< 60 nm) and a high depth resolution (< 1 nm). Therefore its ideally suited for depth profiling applications, as used within this paper. Since the SIMS technique itself relies on the removal of atoms from the surface, it is by its very nature a destructive technique. A depth profile of a sample was obtained by recording sequential SIMS spectra as the surface is gradually sputtered away by the incident ion beam probe. A plot of the intensity of a resulting secondary ion flow signal as a function of time is a direct measure of the variation of its concentration with depth below the surface.

The time of flight based SIMS instrument (Ion-TOF) with high energy Bi^+ primary source was employed for the structural analysis of the devices. For structure depth profiling high energy pulsed primary source (25 keV) was combined with low energy sputter guns at 500 eV Cs^+ gun in 45° to sample surface. Sputtering ion beam was rastered over 300 × 300 μm^2 area while the primary beam is used to scan an area of 80 × 80 μm^2 centred in the middle of the sputtered area. Standard spectra were taken from each sample before the surface analysis. In order to compensate the charging effect of the samples, electron flooding was used.

Femtosecond pump-probe experiments were performed using a regeneratively amplified Ti-Sapphire based system (Clark-MXR model CPA-1); the fundamental beam (780 nm, 150 fs) was used directly as pump beam after proper attenuation; another part of the pump beam was used for supercontinuum generation in a sapphire crystal. Detection of the differential transmission spectra was performed using a fast spectrometer (Entwicklungsbüro Stresing GmbH) capable of recording the spectra at 1 kHz repetition rate. Details of the setup can be found elsewhere.[39] Data evaluation and global fitting was performed in Python using the numpy and scipy libraries. In data evaluation, the low signal approximation was used ($\Delta T/T \approx -\Delta A$).

Acknowledgements

We thank Guglielmo Lanzani for providing us access to the ultrafast spectroscopy lab of the Dipartimento di Fisica, Politecnico di Milano. LL thanks the Spanish Ministry of Science and Innovation for a Ramon Y Cayal fellowship and the European Union for Financial Support (Program AMAROUT). The support of this work by the Austrian Center of Competence in Mechatronics (ACCM) is gratefully acknowledged.

Received: December 18, 2012
Published online:

[1] C. J. Brabec, J. A. Hauch, P. Schilinsky, C. Waldauf, *MRS. Bull.* **2005**, *30*, 50.
[2] M. C. Scharber, D. Mühlbacher, M. Koppe, P. Denk, C. Waldauf, A. J. Heeger, C. J. Brabec, *Adv. Mat.* **2006**, *18*, 789.
[3] D. Mühlbacher, M. Scharber, M. Morana, Z. Zhu, D. Waller, R. Gaudiana, C. Brabec, *Adv. Mat.* **2006**, *18*, 2884.
[4] A. B. Tamayo, X.-D. Dang, B. Walker, J. Seo, T. Kent, T.-Q. Nguyen, *Appl. Phys. Lett.* **2009**, *94*, 103301.
[5] J. Hou, H.-Y. Chen, S. Zhang, G. Li, Y. Yang, *J. Am. Chem. Soc.* **2008**, *130*, 16144.
[6] Y. Liang, Y. Wu, D. Feng, S.-T. Tsai, H.-J. Son, G. Li, L. Yu, *J. Am. Chem. Soc.* **2009**, *131*, 56–57.
[7] M. M. Wienk, M. P. Struijk, R. A. J. Janssen, *Chem. Phys. Lett.* **2006**, *422*, 488.
[8] B. P. Karsten, R. A. J. Janssen, *Org. Lett.* **2008**, *10*, 3513.
[9] M. M. Wienk, M. G. R. Turbiez, M. P. Struijk, M. Fonrodona, R. A. J. Janssen, *Appl. Phys. Lett.* **2006**, *88*, 153511.
[10] Y. Yao, C. Shi, G. Li, V. Shrotriya, Q. Pei, Y. Yang, *Appl. Phys. Lett.* **2006**, *89*, 153507.
[11] H.-G. Flesch, R. Resel, C. R. McNeill, *Org. Electronics* **2009**, *10*, 1549–1555.
[12] E. M. J. Johansson, A. Yartsev, H. Rensmo, V. Sundström, *J. Phys. Chem. C* **2009**, *113*, 3014–3020.
[13] M. Koppe, H.-J. Egelhaaf, G. Dennler, M. C. Scharber, C. J. Brabec, P. Schilinsky, C. N. Hoth, *Adv. Funct. Mater,.* **2010**, *20*, 338–346.
[14] T. Ameri, J. Min, N. Li, F. Machui, D. Baran, M. Forster, K. J. Schottler, D. Dolfen, U. Scherf, C. J. Brabec, *Adv. Energy Mater.* **2012**, *2*, 1198.
[15] N. Li, F. Machui, D. Waller, M. Koppe, C. J. Brabec, *Sol. Energy Mater. Sol. Cells* **2011**, *95*, 3465.
[16] F. Machui, S. Rathgeber, N. Li, T. Ameri, C. J. Brabec, *J. Mater. Chem.* **2012**, *22*, 15570.
[17] M. C. Scharber, M. Koppe, Jia Gao, F. Cordella, M. A. Loi, P. Denk, M. Morana, H.-J. Egelhaaf, K. Forberich, G. Dennler, R. Gaudiana, D. Waller, Z. Zhu, X. Shi, C. J. Brabec, *Adv. Mat.* **2010**, *22*, 367.
[18] D. Mühlbacher, M. Scharber, M. Morana, Z. Zhu, D. Waller, R. Gaudiana, C. Brabec, *Adv. Mater.* **2006**, *18*, 2884.
[19] H. Löslein, T. Ameri, G. J. Matt, M. Koppe, H.-J. Egelhaaf, A. Troeger, V. Sgobba, D. M. Guldi, C. J. Brabec, **2012**, Unpublished.
[20] F. Padinger, R. S. Rittberger, N. S. Sariciftci, *Adv. Funct. Mater.* **2003**, *13*, 85.
[21] K. Dalnoki-Veress, J. A. Forrest, J. R. Stevens, J. R. Dutcher, *Physica A* **1997**, *239*, 87.
[22] G. Li, Y. Yao, H. Yang, V. Shrotriya, G. Yang, Y. Yang, *Adv. Funct. Mat.* **2007**, *17*, 1636.

© 2013 WILEY-VCH Verlag GmbH & Co. KGaA, Weinheim

[23] J.-F. Chang, B. Sun, D. W. Breiby, M. M. Nielsen, T. I. Sölling, M. Giles, I. McCulloch, H. Sirringhaus, *Chem. Mat.* **2004**, *16*, 4772.
[24] D. M. DeLongchamp, B. M. Vogel, Y. Jung, M. C. Gurau, C. A. Richter, O. A. Kirillov, J. Obrzut, D. A. Fischer, S. Sambasivan, L. J. Richter, E. K. Lin, *Chem. Mat.* **2005**, *17*, 5610.
[25] M. Geoghegan, G. Krausch, *Prog. in Polym. Science* **2003**, *28*, 261.
[26] S. Y. Heriot, R. A. L. Jones, *Nat. Mat.* **2005**, *4*, 782.
[27] M. Sprenger, S. Walheim, A. Budkowski, U. Steiner, *Interface Science* **2003**,*11*, 225.
[28] J.-B. Lhoest, P. Bertrand, L. T. Weng, J.-L. Dewez, *Macromol.* **1995**, *28*, 4631.
[29] C. M. Björström, S. Nilsson, A. Bernasik, A. Budkowski, M. Andersson, K. O. Magnusson, E. Moons, *Appl. Surf. Sci.* **2007**, *253*, 3906.
[30] J.-S. Kim, P. K. H. Ho, C. E. Murphy, R. H. Friend, *Macromol.* **2004**, *37*, 2861.
[31] J. Chappell, D. G. Lidzey, P. C. Jukes, A. M. Higgins, R. L. Thompson, S. O'Connor, I. Grizzi, R. Fletcher, J. O'Brien, M. Geoghegan, R. A. L. Jones, *Nat. Mat.* **2003**, *2*, 616.
[32] A. C. Arias, N. Corcoran, M. Banach, R. H. Friend, J. D. MacKenzie, W. T. S. Huck, *Appl. Phys. Lett.* **2002**, *80*, 1695.
[33] G. Grancini, N. Martino, M. R. Antognazza, M. Celebrano, H.-J. Egelhaaf, G. Lanzani, *J. Phys. Chem. C* **2012**, *116*, 9838–9844.
[34] I.-W. Hwang, C. Soci, D. Moses, Z. Zhu, D. Waller, R. Gaudiana, C. J. Brabec, A. J. Heeger, *Adv. Mater.* **2007**, *19*, 2307–2312.
[35] I. A. Howard, R. Mauer, M. Meister, F. Laquai, *J. Am. Chem. Soc.* **2010**, *132*, 14866–14876.
[36] J. Guo, H. Ohkita, H. Benten, S. Ito, *J. Am. Chem. Soc.* **2010**, *132*, 6154–6164.
[37] R. Österbacka, C. P. An, X. M. Jiang, Z. V. Vardeny, *Science* **2000**, *287*, 839–842.
[38] C. Waldauf, M. Morana, P. Denk, P. Schilinsky, K. Coakley, S. A. Choulis, C. J. Brabec, *Appl. Phys. Lett.* **2006**, *89*, 233517.
[39] D. Polli, L. Lüer, G. Cerullo, *Rev. Sci. Inst.* **2007**, *78*, 103108.

© 2013 WILEY-VCH Verlag GmbH & Co. KGaA, Weinheim
Adv. Energy Mater. **2013**,
DOI: 10.1002/aenm.201201076